



Microanisotropy and preferred orientation of grains and aggregates (POGA) of the Malan loess in Yan'an, China: a profile study

Xi'an Li¹ · Bo Hong^{1,2} · Li Wang^{1,2} · Lincui Li¹ · Jianqiang Sun¹

Received: 3 June 2019 / Accepted: 17 November 2019 / Published online: 11 December 2019
© Springer-Verlag GmbH Germany, part of Springer Nature 2019

Abstract

It is well known that the microfabric formed by the shape, size, and preferred orientation of grains and aggregates (POGA) is the primary cause of the macroscopic anisotropy of soil. Therefore, this study investigated the vertical and horizontal anisotropic characteristics of the POGA at different burial depths in the Malan loess of Yan'an. Quantitative information of particle aggregates from scanning electron microscopy (SEM) photographs of vertical and horizontal solidified slice specimens was derived via the ArcGIS vectorization tool. The variation in the roundness (R), anisotropy index (I_a), and probability entropy (H_m) of clay grain aggregates was analyzed, and the results show that the azimuthal of the POGA in the horizontal direction is between 130° and 150° (N 40° W–N 60° W), while the POGA in the vertical direction is parallel to the ground plane. Moreover, the deeper the burial depth is, the more significant the preferred orientation (PO). Both vertical and horizontal grain aggregates are based on rounded grains, and the I_a of soil increases with the burial depth. The H_m shows little change in the horizontal direction with the burial depth but decreases in the vertical direction, and the POGA of the vertical direction is better than that of the horizontal direction. Finally, the I_a and H_m of undisturbed loess are compared with that of remolded clay in the published literature, and the relationship between microanisotropy and POGA is discussed.

Keywords Loess · Microanisotropy · Preferred orientation · Roundness · Anisotropy index · Entropy

Introduction

Developing a correct understanding and description of the anisotropic behavior of undisturbed loess is among the important problems in geotechnical engineering in loess areas. Cagauan and Uehara (1965) defined the anisotropy of soil as the degree of orientation of soil particles and limited it to the optical anisotropy of natural undisturbed soil units. However, for most natural clays, the clay minerals are usually elongate or tabular, and they are always present in the soil as large and small aggregates, with large aggregates capable of containing smaller aggregates (e.g., microaggregates), which

continues until soil is formed (Shi et al. 1998). The microfabric formation of the arrangement of clay grains and aggregates in the soil may be related to the directional dependence, i.e., anisotropy, of the macroscopic physical properties. These anisotropic features are also manifested in various aspects, such as elastic anisotropy (Graham and Houlsby 1983; Lonardelli et al. 2007), thermodynamic anisotropy (Hueckel and Pellegrini 1996), magnetic anisotropy (Sun et al. 1995; Wang et al. 1995; Lagroix and Banerjee 2002), strength anisotropy (Liang et al. 2016; Zhang et al. 2017), deformation anisotropy (Cairncross and James 1977; Karlsson and Karstunen 2017; Xu et al. 2018), and permeability anisotropy (Leroueil et al. 1990; Chapuis and Gill 1989; Henderson and Pena 2017; Hong et al. 2019). Therefore, the study of the soil microfabric (or POGA) is an important perspective for studying the macroscopic anisotropy of soil.

Many pioneering studies on clay grain aggregates and their microfabric orientation indicate that the microfabric is an important cause of soil anisotropy (Cagauan and Uehara 1965; Morgenstern and Tchalenko 1967a, b; Lafeber 1967; Matalucci et al. 1969, 1970a, b; Tovey 1973; Osipov and Sokolov 1978; Hartley 1990; Hicher et al. 2000; Magaldi

✉ Bo Hong
hongbo@chd.edu.cn

¹ School of Geological Engineering and Geomatics, Chang'an University, Xi'an 710064, China

² Key Laboratory of Mine Geological Hazards Mechanism and Control, Shaanxi Institute of Geological Survey, Xi'an 710054, China

et al. 2002; Zhao et al. 2018). Although many attempts have been made to explain the orientation of grain aggregates or microfabrics via polarizing microscopy (Lafeber 1967), X-ray diffraction (XRD) (Brewer and Haldane 1957; Curtis et al. 1980; Zevin and Viaene 1990), scanning electron microscopy (SEM) (Matalucci et al. 1969, 1970a, b; Edil and Krizek 1975), and nuclear magnetic resonance (NMR) (Özarlan and Basser 2008), a quantitative description has not been provided. Tovey (1980) Tovey et al. (1989, 1992a, b; Tovey and Krinsley 1992) presented an index to quantitatively measure and evaluate the orientation of the soil grains and fabric by using an image processing technique, i.e., the index of anisotropy (Ia). Later, Shi et al. (1995, 1998) and Shi (1996) introduced Shannon entropy and proposed two methods for evaluating the order extent of the soil fabric: probability/alignment entropy (Hm) and frequency distribution function. A soil microanisotropy evaluation system has basically been formed (the Tovey-Shi evaluation system), and Shi et al. (1998) used this evaluation system to evaluate the orientation of compacted soil microfabric and its application in a micromechanical model. Wang et al. (2008a, 2010) and Wang (2009) applied the Ia to study the problem of particle orientation in pollutant barrier material and roadbed compacted clay by ArcGIS software. Tang et al. (2012) quantitatively analyzed the orientation of micropores before and after freezing of Shanghai silty clay. Zhang et al. (2017) used Hm to evaluate the strength anisotropy of undisturbed loess and the orientation mechanism of soil particles in Xining, China. Obviously, the Tovey-Shi evaluation system of soil microanisotropy is helpful for understanding the macroscopic anisotropy behavior of soil.

Chinese loess is a kind of aeolian sedimentary clay formed in arid and semiarid climate. Under the alternation of cold and warm paleoclimates, the stratigraphic profile shows distinct anisotropy. In the process of sedimentation and consolidation of the natural soil layer, the transport rate of soil particles and the structural units composed of these particles is slow, and the growth rate of the overlying soil pressure is lower than that of the solidification bonding between particles. Therefore, loess aggregates are often oriented and constitute structural anisotropy. This structure is also an important reason for the anisotropy of the physical properties of loess. In this paper, the orientation characteristics of soil aggregates are reflected by quantitative data, such as the roundness (R), orientation angle (θ), and Ia and Hm, contained in SEM photographs of loess in horizontal and vertical directions with different burial depths, and the anisotropic nature of the loess microfabric is revealed. Undoubtedly, it is of great significance to understand the soil anisotropic behavior from the POGA and promote research on the soil structure.

Materials and image processing

Site description and soil sampling

Chinese loess is famous for its wide distribution, large thickness, complete stratigraphic development, and continuous sedimentary time, and it is mainly distributed between 30°N and 49°N and 75°E and 127°E. The Loess Plateau is most developed from 34°N to 39°N and has a distribution area of approximately 630,000 km². The research site at Yan'an is located in the middle of the Loess Plateau (Fig. 1b), which belongs to an arid-semiarid climate in the midlatitude zone. The upper layer of the late Quaternary aeolian loess was formed approximately 5~10 ka from the present and has a deposition thickness of approximately 10~30 m (Fig. 1c). Because the shallow loess is still underconsolidated and less disturbed by consolidation, the soil particles inherit more of the shape of the initial accumulation. Therefore, we selected shallow loess to study the characteristics of POGA.

The loess used in the experiment was obtained from a fresh section of the Cutting Hills and Filling Land project for the Phase I Project in the Yan'an New Area. The soil samples were manually cut at depths of 2 m, 4 m, 6 m, 8 m, and 10 m below the surface (Fig. 1d). Large cubic clods were excavated from the section (Fig. 1e), and they were then cut into cylindrical soil columns, loaded into a metal bucket, and filled with crushed soil in situ to prevent breakage. The orientation was calibrated by compass, and the score was marked on the top of the soil column. The sample information was recorded on the label, and then the container was sealed with plastic tape and returned to the laboratory (Fig. 1f). The particle size distribution of the soil samples was determined using a laser particle size analyzer, and the soil was classified by the particle size (Fig. 2a and Table 1). The basic properties of the same soil have been published by Li and Li (2017) and Hong et al. (2019), and the values are shown in Fig. 2b and Table 1.

ω is the natural moisture content; ρ is the natural density; e is the porosity ratio; W_p is the plastic limit; W_L is the liquid limit; I_p is the plaster index

Specimen preparation and photo collection

SEM is an effective method for studying the microstructure of soil. SEM surveys have also been widely used to study the POGA. However, the preparation of soil microsamples is a relatively complex process, and the quality of sample preparation directly determines whether the SEM photos can truly reflect the microfabric characteristics of the soil. Generally, soil microsamples can be divided into two categories according to the observed surface conditions. (a) The first category is relatively flat surfaces (Fig. 3a), such as splitting/fracture surfaces (Delage and Lefebvre 1984; Hicher et al. 2000; Liu et al. 2011; Hattab et al. 2013; Nguyen et al. 2014). Although the

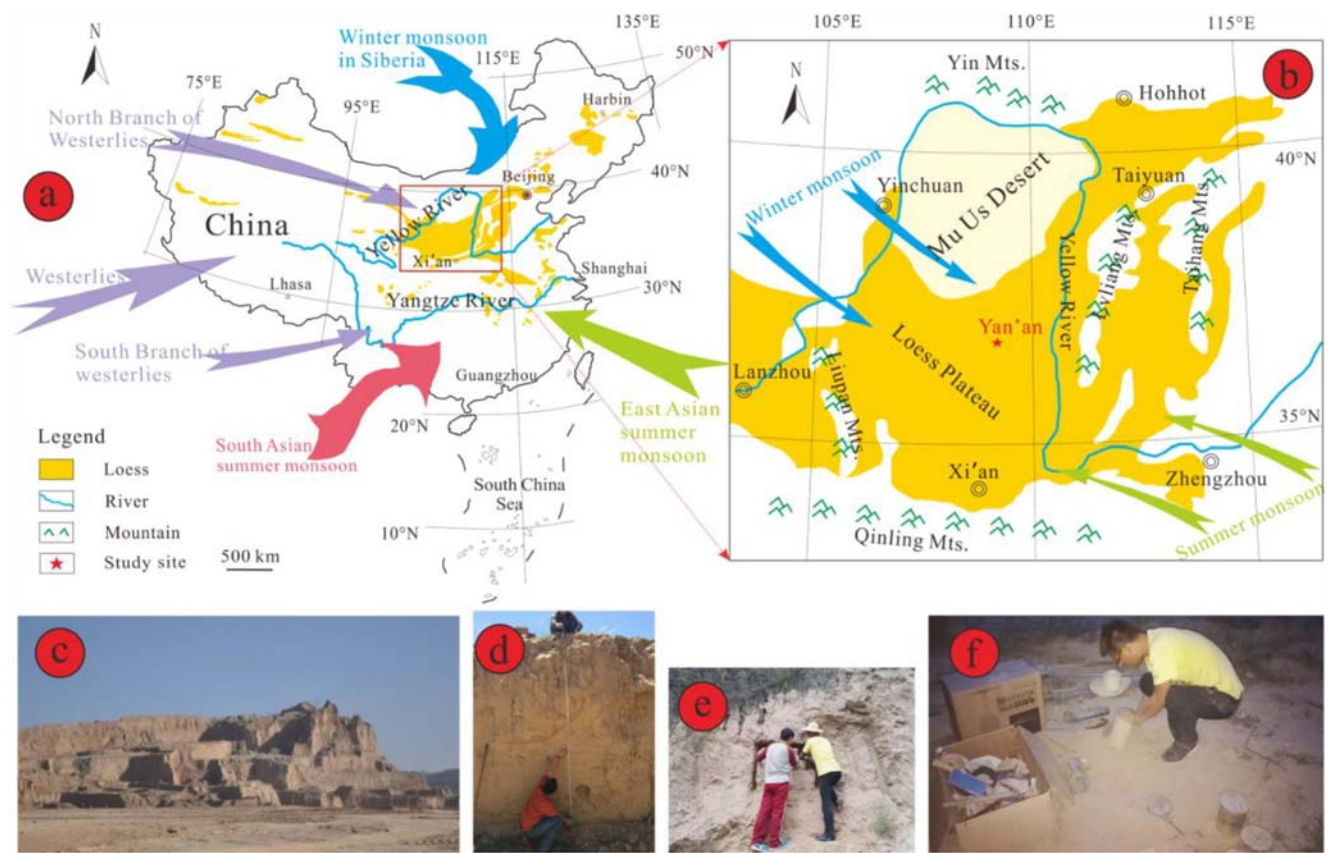


Fig. 1 Regional investigation and sampling process: (a) distribution of loess in China and prevailing wind direction of the Loess Plateau (Zhang et al. 2010); (b) location of Yan'an; (c) engineering site; (d) depth survey;

(e) excavation of block samples; and (f) manual sampling and marking and sealing of the samples

authors attempt to prepare a flat observation surface, this method will inevitably lead to the separation of some particles from the original section (Wang 2009), and it will also disturb the adjacent microfabric. In addition, the observation surface of the split/fracture surface under the microscope is uneven, and the microscopic photographs have a certain field depth.

Therefore, the particle/pore boundary is difficult to define, which makes the postprocessing of SEM photographs more difficult and leads to deviations in microscopic statistics. (b) The second category is solid-sliced surfaces (Fig. 3b). In addition to the relatively time-consuming curing process, this method almost completely avoids the disadvantages of the

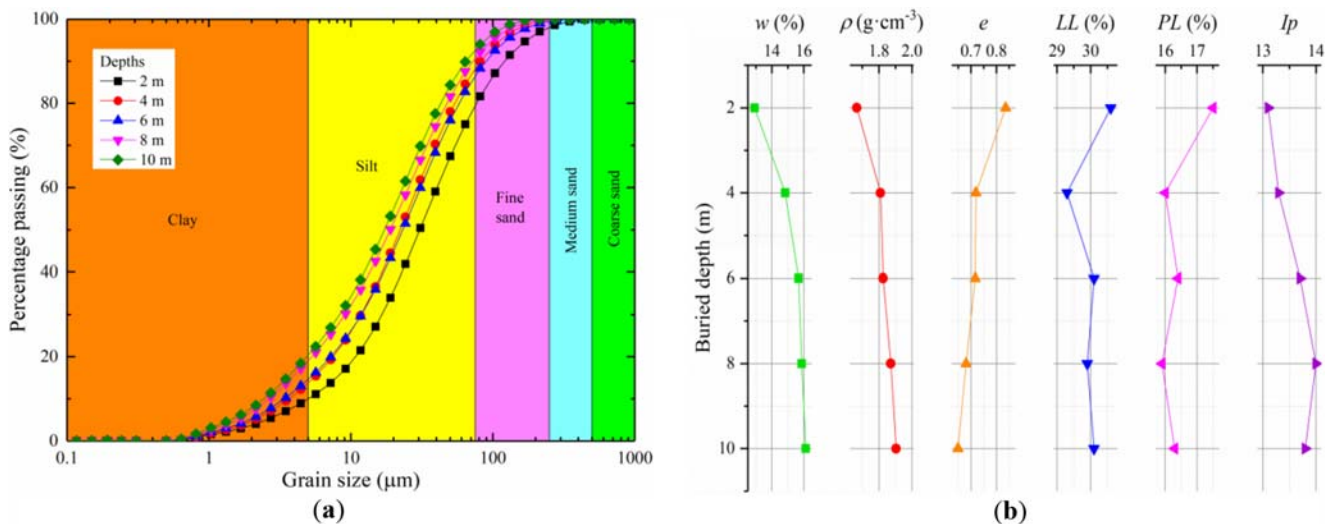


Fig. 2 Soil description: (a) particle size distribution and classification and (b) properties of the Yan'an Malan loess

Table 1 Basic properties of the samples

Depth (m)	ω (%)	ρ (g/cm ³)	e	W_p (%)	W_L (%)	I_p	Clay <5 μm	Silt 5~75 μm	Fine sand 75~250 μm	Medium sand 250~500 μm	Coarse sand >500 μm
2	12.9	1.67	0.836	17.5	30.6	13.1	10.00	69.51	18.50	1.99	-
4	14.8	1.81	0.719	16.0	29.3	13.3	13.83	74.31	11.66	0.20	-
6	15.7	1.83	0.717	16.4	30.1	13.7	14.67	71.72	13.05	0.56	-
8	16.1	1.87	0.681	15.9	29.9	14.0	19.04	71.62	9.34	0.08	-
10	15.9	1.90	0.649	16.3	30.1	13.8	20.45	72.20	7.35	-	-

first method, and its advantages are obvious; therefore, it is also widely used in soil microstructure research (e.g., Morgenstern and Tchalenko 1967a, b; Lafeber 1967; Matalucci et al. 1969, 1970a, b; Liu et al. 2015; Li and Li 2017; Li et al. 2018).

Therefore, the solid-sliced sample preparation method was adopted in this study. The impregnating solution of the curing treatment was prepared with epoxy resin (cementing agent), acetone (diluent), ethylenediamine (curing agent), and dibutyl phthalate (plasticizer) at a volume ratio of 60:30:4:1. The specific operation steps of the curing treatment have been published by Li and Li (2017) and Li et al. (2018) to study the loess microstructure. The preparation process of the microsamples and image acquisition using a Quanta FEG 450 scanning electron microscope are shown in Fig. 4.

Image postprocessing

Graphic vectorization is one of the basic functions of ArcGIS, which was used to process the SEM photographs and has been used in the study of the microstructure pore/particle fractals of cohesive soil (Wang et al. 2004, 2007) and three-dimensional reconstruction and visualization (Wang et al. 2008b) and orientation of clay particles (Wang et al. 2008a, 2010; Wang 2009). Wang et al. also provided a detailed introduction on the use of ArcGIS to process SEM photographs (Wang et al. 2008a, 2010; Wang 2009) and used SEM photographs with high and low undulation (split/fracture surface) to study the soil microstructure features. In this study, ArcGIS 10.2 (ESRI 2013) software was used as a vectorization tool to process the

solid-sliced SEM images to study the POGA in the same profile with depth.

The image postprocessing flow is shown in Fig. 5. The ArcGIS vectorization tool is used to convert the SEM image into vector polygons. Classification was conducted according to the particle size (Fig. 1a), and incomplete particles along the edges of photos were removed. The area, perimeter, maximum diameter (d_{\max}), minimum diameter (d_{\min}), and θ of each particle were statistically obtained. The rose pattern of the POGA is drawn according to the θ , and the long axis (Dmax) and the short axis (Dmin) as well as the principal θ of the best fitting ellipse of the rose chart were obtained by using the standard deviation ellipse principle of the ArcGIS toolbox.

Statistical methods

Roundness (R)

R is a shape factor that is a widely used two-dimensional shape measurement method and an important indicator of particle shape. For a circle, its R has a maximum value of 1, and for a shape with a low ratio area (A) to perimeter (P), such as a narrow or thin shape or a rough-edged shape, its R value is less than 1 (Arasan et al. 2011). Cox (1927) initially defined a two-dimensional R , which is easy to measure according to the concept of three-dimensional objects' sphericity. That is, R is the degree to which the ratio of the area to the circumference approaches the same ratio for a circle, and its expression is shown in Eq. (1):

Fig. 3 Comparison of two microsamples under the microscope: (a) splitting/fracture surfaces and (b) solid-sliced surfaces

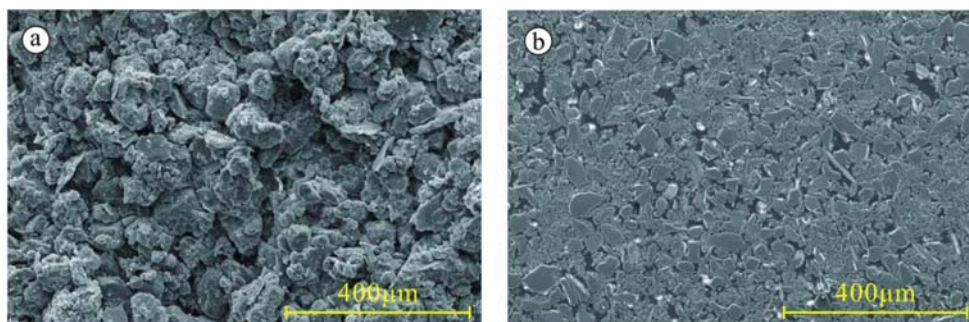


Fig. 4 Microsample preparation process and SEM photo collection: **(a)** sample drying and cutting small cylinders; **(b)** impregnating the sample under low pressure generated by a vacuum pump; **(c)** cutting off the excess part of the specimen; **(d)** Transferring the specimen to the impregnation mold; **(e)** lapping and polishing the impregnated sample with sandpaper and polishing agent, respectively; **(f)** filming the SEM photo by the Quanta FEG 450; and **(g)** obtaining SEM photos

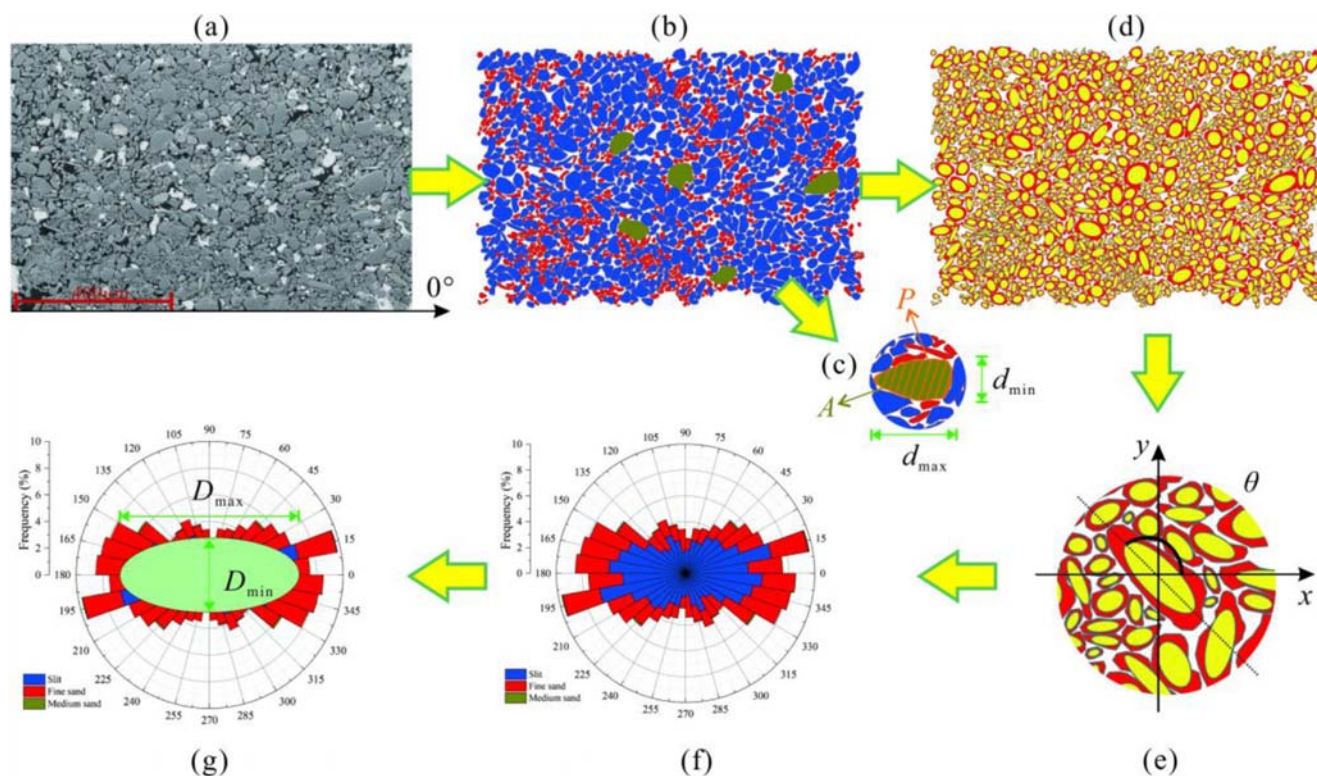
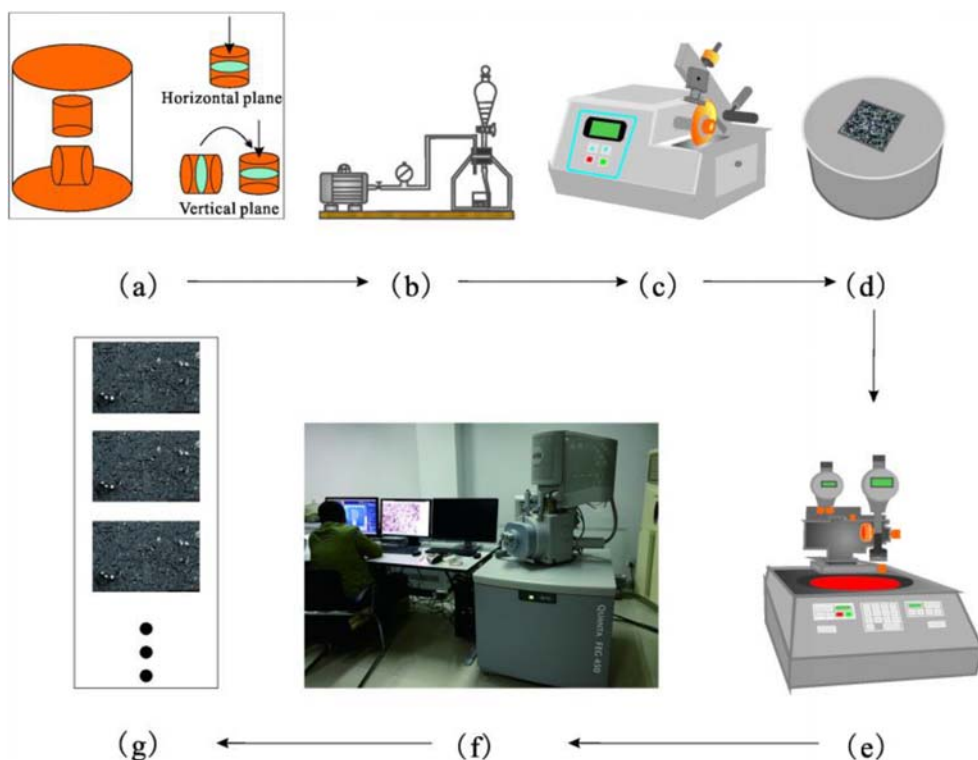


Fig. 5 ArcGIS image postprocessing flow: **(a)** original SEM image; **(b)** using ArcGIS to convert SEM images into vector polygons and classify the polygons; **(c)** extracting morphological data of the particles, including the area, perimeter, maximum diameter, and minimum diameter; **(d)**

drawing standard deviation ellipse of particles; **(e)** obtaining the orientation angle; **(f)** plotting the azimuth rose diagram; and **(g)** determining the general direction and anisotropy parameters of soil using a standard deviation ellipse

$$R = \frac{4\pi A}{P^2} \quad (1)$$

Anisotropy index

To reflect the overall orientation of the soil microfabric, Tovey (1980) defined I_a as the ratio of the principal axis to the minor axis of the optimal fitting ellipse of the rose diagram of the soil fabric orientation distribution and used this ratio to reflect the degree of soil fabric anisotropy (D_{\max}/D_{\min}). Later, Tovey et al. (1989) improved the above definition as $(1 - d_{\min}/D_{\max})$, which was used by Tovey and Krinsley (1990) and Tovey et al. (1992a, b) to perform a directional analysis of fine minerals and micropores in soil and sediments. Shi et al. (1995, 1998), Shi (1996) and Wang et al. (2008a) applied this improved formula to study the orientation of clay microscopic fabric (grain or pore). Therefore, the definition of I_a adopted in this study is shown in Eq. (2):

$$I_a = \frac{d_{\max} - d_{\min}}{d_{\max}} \times 100\% \quad (2)$$

Probability/alignment entropy

The I_a reflects the overall distribution of the cohesive soil microfabric to a certain extent, but it does not reflect the orderliness of the body of the fabric unit. Shi et al. (1995, 1998) and Shi (1996) introduced Shannon entropy to reflect the orderliness of the arrangement of the microscopic structural units of the clay, called H_m (probability entropy or alignment entropy). Liu et al. (2011) and Zhang et al. (2017) also used this index to quantitatively evaluate the degree of order of microscopic pores in clay materials. H_m is defined as shown in Eq. (3):

$$H_m = - \sum_{i=1}^n \frac{m_i}{M} \cdot \frac{\ln(m_i/M)}{\ln n} = - \sum_{i=1}^n P_i \cdot \log_n P_i \quad (3)$$

where H_m is the probability entropy of the arrangement of cohesive soil structural units, m_i is the number of particles in the i -th azimuthal zone, M is the total number of particles, and n is the number of azimuthal zones equally divided in the direction of the unit arrangement. The arrangement direction is 0° – 180° , which is equally divided into 10° sections, with $n = 18$. P_i is the probability that the structural unit occurs in a certain azimuth.

Results and discussion

Variation in the roundness (R) with depth and its correlation with anisotropy

Many kinds of R classifications of particles have been developed according to different research purposes and research

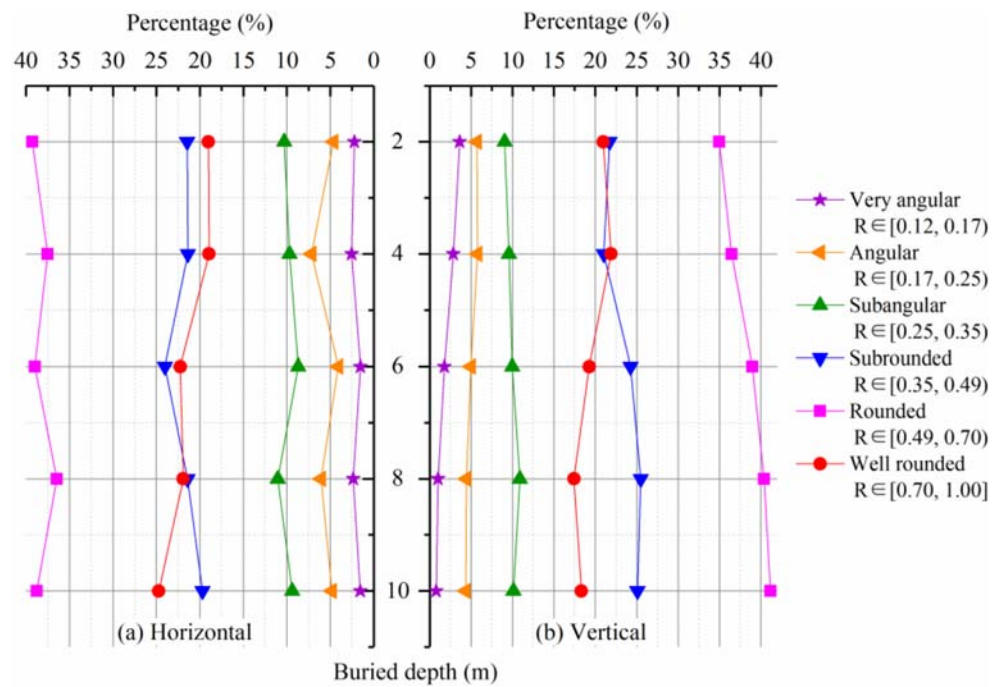
methods (Russell and Taylor 1937; Krumbein 1941; Powers 1953; Alshibli and Alsaleh 2004; Al-Rousan et al. 2007; Arasan et al. 2011). Based on the R value of Eq. (1), the R classification of Powers (1953) will be adopted in this paper. Powers believes that the angular group in the Russell and Taylor (1937) five-group classification should be subdivided and that a set composed of very angular particles should be added; therefore, the R of the particles can be divided into six categories.

Figure 6 shows that the rounded particle content is dominant in both vertical and horizontal soil aggregates. In the horizontal direction, the content of very angular, angular, and subangular particles changed little as the depth increased (by approximately 2.5%, 5%, and 10%, respectively), while the content of subrounded and rounded grains decreased slightly, and the number of well-rounded particles increased slightly. In the vertical direction, the variation in the angular and subangular grain contents was similar to the variation in the horizontal direction with increases in depth, and the contents were approximately 5% and 10%, respectively. The study of Zhang et al. (2017) also showed that undisturbed loess particles are mainly round or elliptical particles that are parallel to the natural sedimentary surface, which is consistent with the results of this study.

Relative frequency percentages of silt, fine sand, and medium sand grains in the various R classes of the aeolian sediments at different depths in horizontal and vertical directions studied are presented in histograms (Fig. 7). In the medium sand group, approximately 60–90% of the grains are rounded and well rounded, 10%–25% are subrounded, while very few are subangular, angular and very angular. In the fine sand group, approximately 55–75% of the grains are rounded and well rounded, 16–28% are subrounded, and approximately 10% are subangular, angular, and very angular. In the silt group, 55–63% of the grains are rounded and well rounded, approximately 18–25% are rounded, and approximately 20% are subangular, angular, and very angular. All of the studied sediments of silt and fine sand have a unimodal distribution with an R class that varies from rounded to angular. However, obvious differences are recognized between histograms of the R classes of the various size fractions. However, mainly subcircular, circular, and very circular sediments were observed, and these shapes mainly depended on the size fraction. Little variation was observed in the frequency distribution of the R classes of medium sand (less than 2%).

Although R cannot directly reflect the anisotropy of the soil, it can control the anisotropy through the morphology, physical properties, contact mode, and POGA. Related studies have also shown that the shape of the particles during the deposition process seriously affects the contact pattern, orientation and anisotropy of the soil particles under the action of gravity (Matalucci et al. 1969). Moreover, round particles have greater shear stiffness (Manne and Devarakonda 2016) and lower stress state sensitivity than particles with other

Fig. 6 Roundness classification and its variation with depth: (a) parallel to the depositional plane (horizontal direction) and (b) perpendicular to the depositional plane (vertical direction)



shapes (Cho et al. 2006). Thus, elongated particles in particular present more pronounced anisotropy than angular or round particles (Nouguier-Lehon et al. 2003).

Many studies have shown that the R of soil particle aggregates can indicate tectonic disturbances and reflect the sedimentary history of soil (Powers 1953) and it also has a controlling effect on the macroscopic physical properties of soil (Nouguier-Lehon et al. 2003; Ting et al. 1995; Kock and Huhn 2007; Alan et al. 2007; Li 2013; Li et al. 2013b). Among these properties, the relationship between the particle's R and internal friction angle is important. The R of sand has a good linear relationship with the internal friction angle (Cho et al. 2006; Sivakumar et al. 2002; Santamarina and Cho 2004; Rousé 2005; Rousé et al. 2008), and clay-gravel mixed soil also has a similar linear relationship (Li 2013; Li et al. 2013b). However, for natural aeolian sediments, anisotropy was generated during the deposition process, and the POGA after deposition will also be affected by the positive correlation of the overburden pressure (Meade 1965), which will lead to a further increase in the directional dependence of the macroscopic physical properties of the soil.

Orientation angle change with burial depth

Since the directional orientation of the unit is mirror symmetrical within the range of 0–360°, only the orientation of the units in the range of 0–180° must be statistically analyzed. The 0–180° range is divided into 18 azimuths of 10° each, and the frequency of the particles in each section is determined. The degree of orientation of the micro unit in each subarea is

determined to obtain an azimuth rose diagram that reflects the directional distribution of the units.

At all depths horizontal and vertical to the photomicrograph of the rose diagram, the grain aggregates have a certain degree of preferred orientation (Fig. 8).

Horizontal direction

The histograms of the preferred orientation of the five horizontal micrographs have a distinct bimodal distribution, although this bimodal distribution remains to be further interpreted (Matalucci et al. 1969). Nevertheless, the preferred direction of the Yan'an Malan loess to the particles is generally between 130° and 150° (N40°W and N60°W), and the probability in this range is greater than 50%, although the maximum probability is only 56.82% (Fig. 8a, c, e, g, i). However, this phenomenon of uniformity of more than 50% at all depths likely indicates that the particles followed a certain regularity in the deposition process, which is similar to the aeolian genesis of Chinese loess. Many studies on Quaternary loess indicate that Chinese loess is the product of dust accumulation from the East Asian winter monsoon during the Quaternary glacial periods (Jing 1980; Li 1986; Wang 1987; An et al. 1991a, b; Pang 1999; Zhang 2001). The main provenance of this dust is Southern Mongolia and the adjacent Gobi and desert areas (Rutter 1992; Sun 2004), and it is mainly carried by near-surface winds (generally below 3000 m) (Zhang 2001; Sun 2004). In particular, the Late Pleistocene loess strongly reflects the close relationship with the Quaternary East Asian paleomonsoon (winter monsoon) climate (Fig. 1a) (Teng and Shen 1995; Ding and Yu 1995; Lu

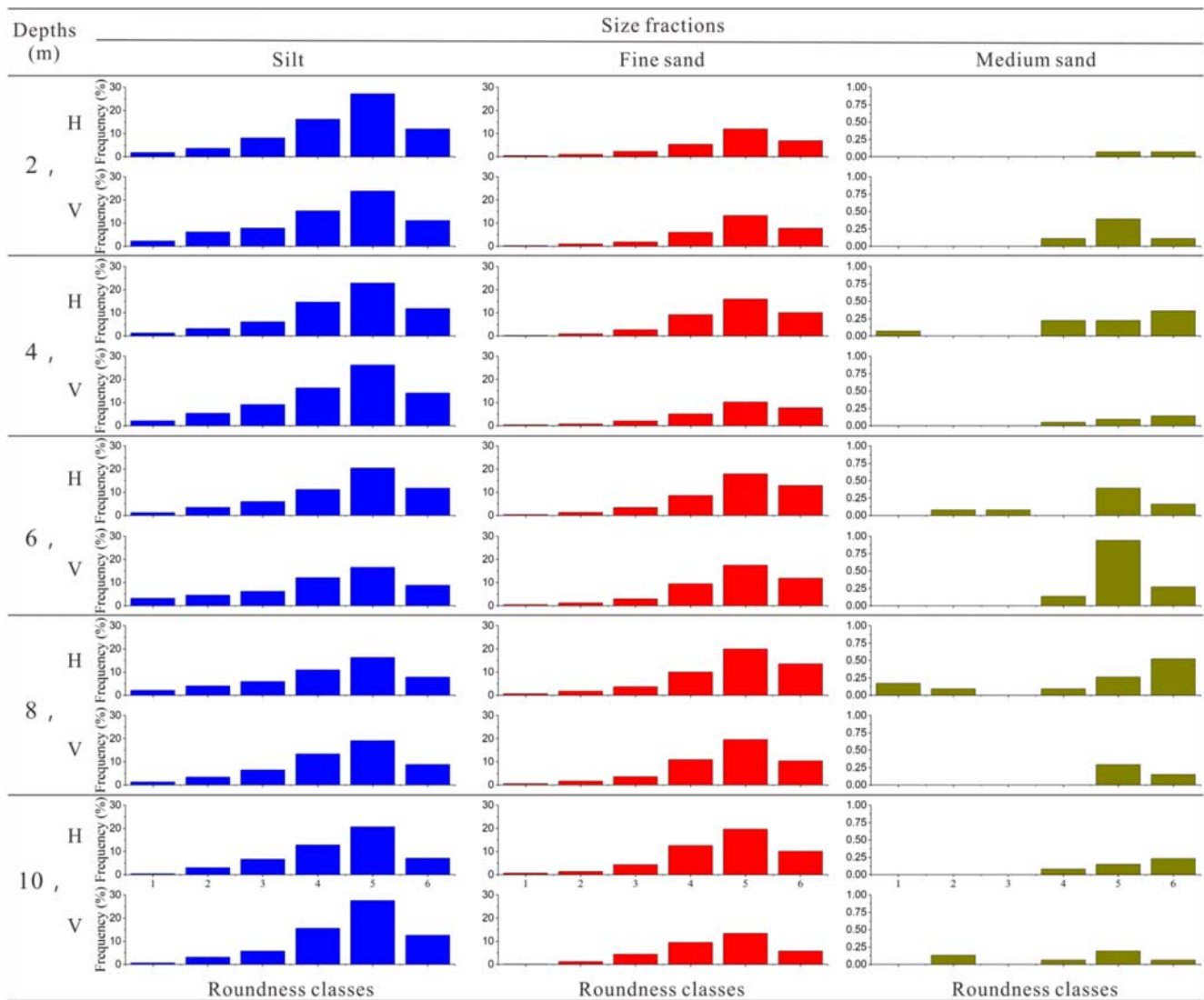


Fig. 7 Histograms of the relative frequency percentages of the roundness classes in the grain-size fractions of the studied sediments. The abscissa is the roundness classification: 1 very angular, 2 angular, 3 subrounded, 4

subrounded, 5 rounded, and 6 well rounded. The number in the first column represents the depth of the soil, H represents the horizontal direction, and V represents the vertical direction

and An 1997, 1998; Sun et al. 1995; Pang 1999; Zhao et al. 2002; Xu et al. 2006; Zhang et al. 2010). This finding is mainly due to the cold climate of the Quaternary glacial period and the difference in the thermal properties between the land and sea, which led to a stronger winter monsoon than summer monsoon in East Asia. At that time, the Mongolian-Siberian region had low temperatures and high air pressure; the pressure gradient was larger, and the wind was stronger than those in the surrounding area. The winter monsoon controlled the climate in northern China for 8–9 months (Ding and Yu 1995). The front could reach the Yangtze River Basin (Pang 1999) and was capable of carrying a large amount of dust deposits over the Loess Plateau (Jing 1980). The summer monsoon in East Asia comes from the ocean. During the Quaternary, the East Asia region was generally hot, the temperature difference was small, the pressure gradient was small, and the East Asian

summer monsoon circulation was very weak, and its activity range was limited to the south of the southern margin of the Loess Plateau (Sun et al. 1996). In addition, the summer monsoon's effect on East Asia was also very short (Ding and Yu 1995) because of the Quaternary glacial climate, which was dry and with little rain; therefore, dry deposition was the main process of dust settlement in the loess area (Zhang 2001). Therefore, a large amount of accumulated loess could be preserved and continued to thicken (Jing 1980; Sun et al. 1996), which preserve the orientation of the particles to some extent (Sun et al. 1995). The direction of the long axis of the particles when the dust material was stacked was parallel to the dominant wind direction (Reading 1978; Sun et al. 1995; Wang et al. 1995). The East Asian winter monsoon prevailed in the Malan loess deposit period in the Loess Plateau, which coincided with the phenomenon that the particles were

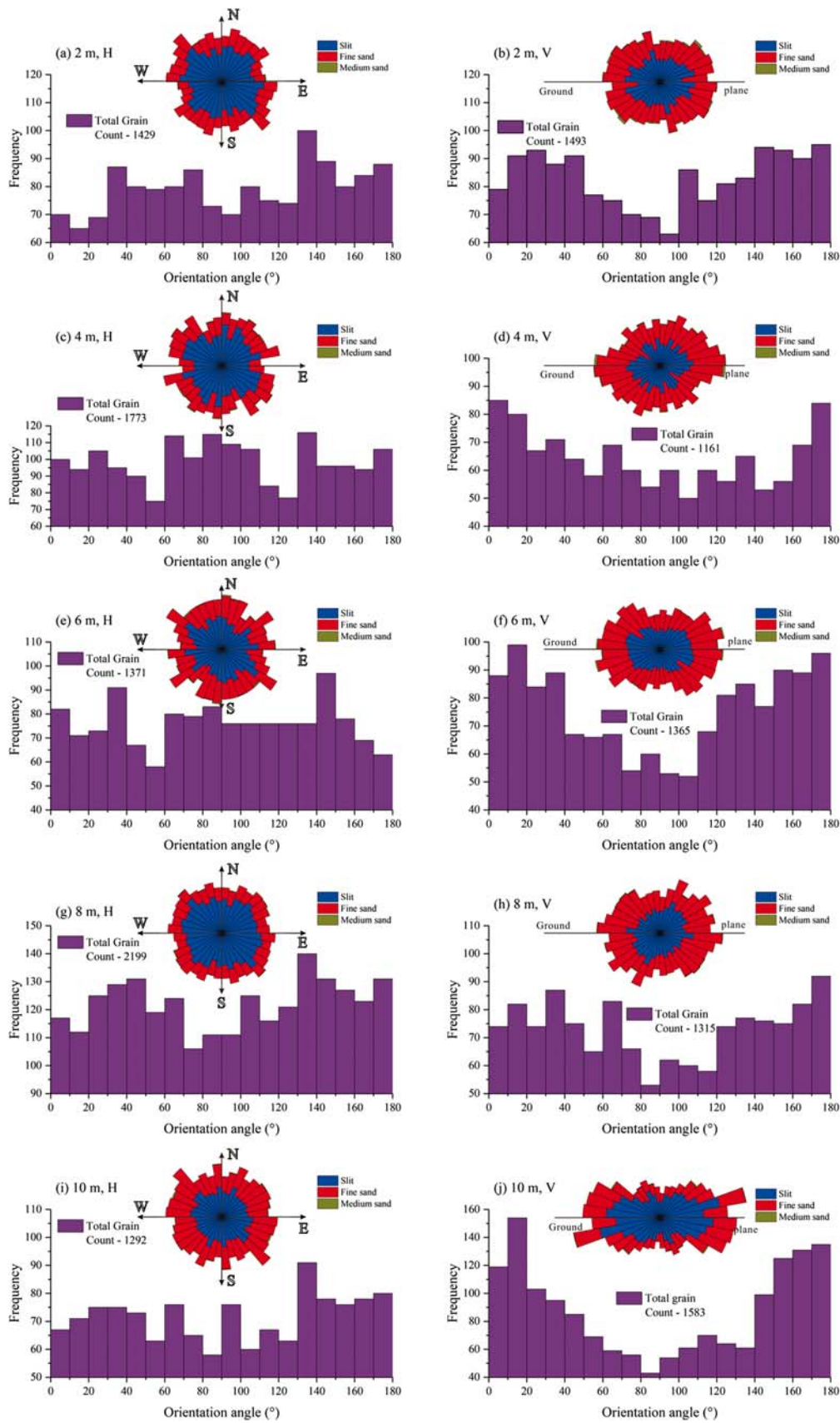


Fig. 8 Horizontal and vertical orientation angle rose diagram and its frequency distributions at different depths (m represents the burial depth, H represents the horizontal direction, and V represents the vertical direction)

distributed horizontally in the slices at all depths. Although it is a weak fit, this result does not completely obscure the fact that the horizontal orientation of the particles likely occurred due to the paleowind direction. Matalucci et al. (1969) studied microscopic photographs of Vicksburg loess and former Vicksburg loess in Mississippi, USA, and showed that the preferred orientation of silt-sized particles preserved the local paleowind direction quite well. Lagroix and Banerjee (2002) also confirmed that the loess fabric in Alaska well recorded the paleowind changes in that area. In addition, this weak coincidence phenomenon (or bimodal distribution of the preferential orientation of particles) may also be due to the local variation in sedimentary wind direction caused by topography, atmospheric turbulence, or other meteorological factors (Matalucci et al. 1969; Wang et al. 1995). Obviously, for the aeolian loess in the Loess Plateau, where the climate is not conducive to the development of loam formation (Lagroix and Banerjee 2002), the loess of POGA in this region should also provide a good indication of the paleowind. If this rule can be verified by loess sections in different areas of the Loess Plateau, then it will be of great significance for both the genesis of loess and the study of paleoclimate.

Vertical direction

The preferred orientation of particles in the five vertical micrographs is substantially within 45° of the ground level (Fig. 8b, d, f, h, j). With increases in depth, the compaction effect increases, and this orientation is more significant. This phenomenon obviously indicates that the particles tend to form a more stable planar structure under the action of gravity and compaction during the deposition process; that is, the maximum axial plane of the particles always tends to adjust or rotate perpendicular to the direction of the maximum principal stress (Cetin 2004; Nougier-Lehon et al. 2003; Kock and Huhn 2007; Hattab and Fleureau 2011). Many researchers have also confirmed that this preferred orientation of particles plays an important role in the formation of anisotropic structures in clay. For example, the results of Cetin (2004) show that the overburden earth pressure may cause a certain degree of preferential orientation. When the overburden earth pressure is less than the maximum effective (preconsolidation) stress, only small preferential orientations and small changes in soil structure will be observed. When the earth pressure is loaded to a stress level greater than the preconsolidation stress, the soil structure is rearranged or orientated into a new more stable and compact structure, which tends to be perpendicular to the direction of the maximum principal stress, and as the load increases, the degree of preferential orientation will increase, thus forming an anisotropic structure. Curtis et al. (1980) argue that the preferred orientation of particles in clay-rich sediments is almost entirely from compaction strain, although the presence of nonplanar particles also prevents the

development of nearby planar structures. Hattab and Fleureau (2011) believe that when the consolidation stress reaches a certain position (under the triaxial path), the rotation mechanism of the particles to the preferential plane becomes more important. Obviously, the preferred orientation of vertical particle agglomerates is caused by compaction strain of clay particles and rotation of nonplanar particles, and this phenomenon is consistent with the macroanisotropy behavior of clay, which is controlled to a large extent by the directional dependence of its microfabric. In particular, the POGA has a very significant influence on the anisotropic behavior of clay (Matalucci et al. 1970a, b; Edil and Krizek 1975; Sachan 2007; Li et al. 2013a).

Anisotropy index and entropy with burial depth

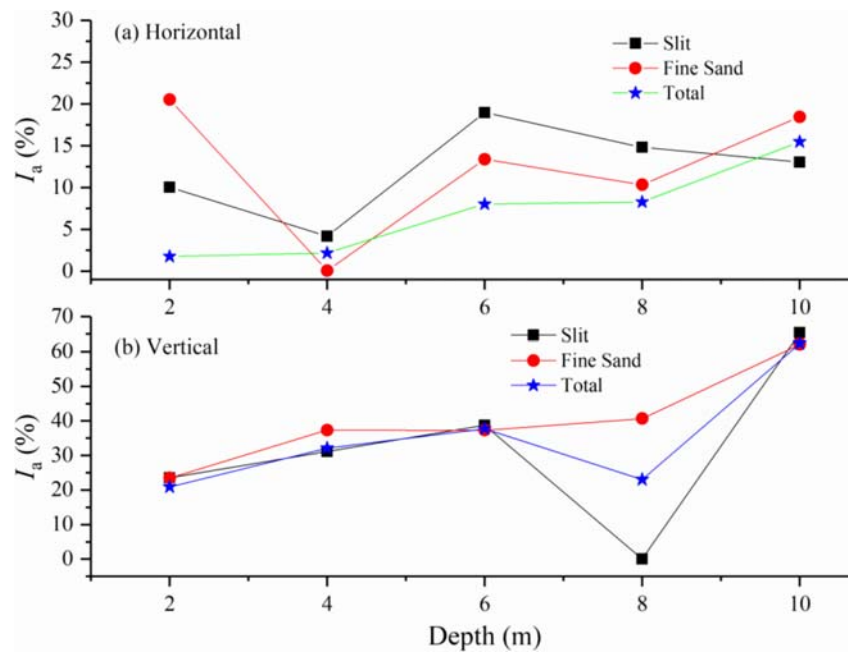
Equation (2) shows that the variation range of I_a can extend from 0 to 100%. When $I_a = 0$, the soil microfabric is random and isotropic overall. When $I_a = 100\%$, the soil microfabric is distributed in the same orientation and completely anisotropic. According to Eq. (3), H_m is in the range of $[0,1]$. When $H_m = 0$, the soil microfabric unit has a certain orientation distribution, which shows that the unit body is oriented and that orderliness is the highest. When $H_m = 1$, the fabric unit probability is the same at each azimuth, indicating complete disorderliness or complete randomness. In other words, larger H_m values correspond to more anisotropic fabrics, while smaller H_m correspond to more isotropic fabrics.

Figure 9a shows that with an increase in depth, the I_a of the silt and fine sand in the horizontal direction is greater than zero, and except for the minimum at 4 m, the I_a at other depths is more than 10%, with a more significant I_a of up to 20.54% observed for fine sand. The total I_a of soil grains gradually increases, with a maximum value of 15.49%. In the vertical direction (Fig. 9b), the I_a of silt, fine sand, and total soil grains increases with the depth of the soil layer. The soil grains have a directional arrangement overall and the anisotropy is remarkable. This finding indicates that as the overburden pressure increases, the clay particles deform or rotate so that the long axis direction of the soil particles tends to be horizontal.

Figure 10 shows that the vertical total H_m values of the different burial depths are smaller than the horizontal values and the order of the vertical grain arrangement is better than that of the horizontal direction. For silt and fine sand, the H_m is > 0.5 for silt and between 0.608 and 0.812 in both the horizontal and vertical directions. For fine sand, the H_m value of fine sand is less than that of silt, and the minimum H_m value is 0.382, which indicates that fine sand tends to be more anisotropic. Thus, fine sand is a good indicator of anisotropy (Matalucci et al. 1969).

Figure 11 shows that I_a and H_m vary with the natural water content. As the water content increases, H_m decreases gradually, I_a increases gradually, and disordered soil fabrics changes

Fig. 9 Variation in I_a with depth: (a) parallel to the depositional plane (horizontal direction) and (b) perpendicular to the depositional plane (vertical direction)

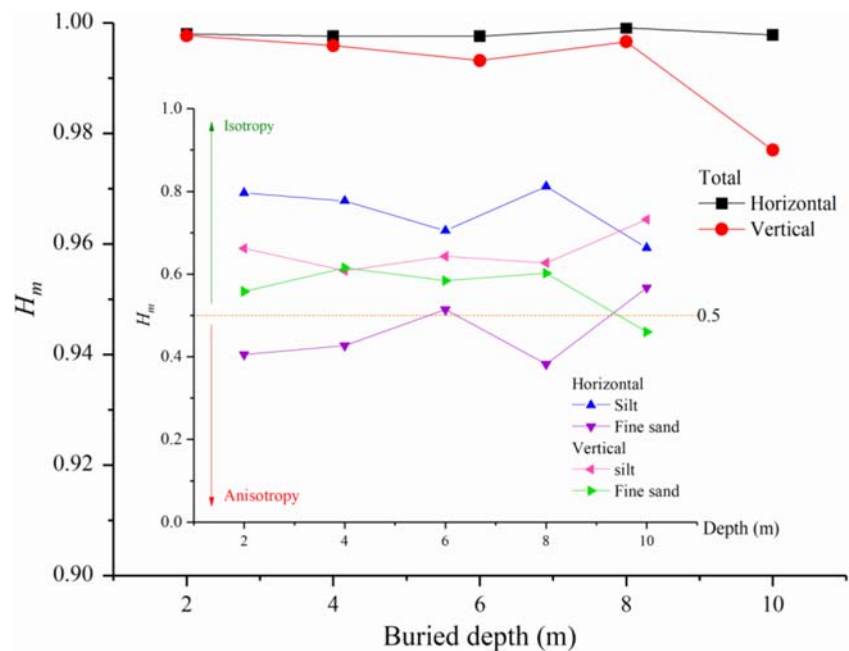


toward ordered fabrics (directional fabrics), although this change relationship is not linear (Shi et al. 1998). When the moisture content was <15.8%, H_m showed little change (Fig. 11a), although the vertical direction had higher I_a than the horizontal direction and the vertical direction had more obvious directional soil arrangement characteristics overall, which increased along with the water content. When the water content exceeded this value, H_m in the vertical and horizontal directions decreased rapidly, and I_a increased rapidly (Fig. 11a). In other words, the ordering of the soil fabric increased,

the directional soil arrangement characteristics became more obvious overall, and the anisotropy became more significant.

Compared with Shi et al. (1998), who performed a one-dimensional compression test of highly plastic expansive clay, the variation in I_a and H_m of the undisturbed loess and the compacted clay was similar to the variation in the water content (Fig. 11b). The difference was only caused by the difference in the threshold water content and consolidation pressure determined by the soil properties. When the consolidation pressure and water content increased to a certain value, the

Fig. 10 Variation in H_m with depth



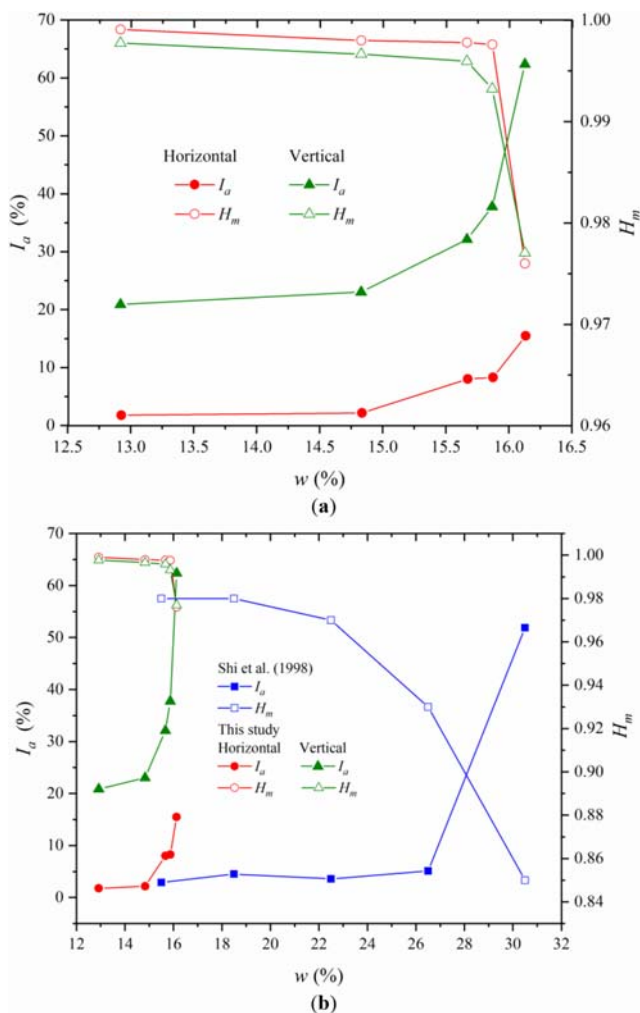


Fig. 11 Changes in I_a and H_m with the water content (w): **(a)** this study and **(b)** compared with Shi et al. (1998)

orientation characteristics of clay particle agglomerates became more apparent (Shi et al. 1998), thus causing anisotropy in the soil (Sivakumar et al. 2002). In addition, the orderly degree of soil fabric more directly indicated the stress-strain state of the soil and the external forces acting on it. Therefore, further study on the variation in I_a and H_m with stress and strain will be of great significance for understanding the physical and chemical properties of fine-grained soil (Shi et al. 1998) because they reflect both the direction of the soil and the order of the soil fabric.

Summary and conclusions

Based on the above analysis results, the following conclusions can be drawn.

The statistical results of R show that the undisturbed loess grains are dominated by rounded grains in directions parallel and perpendicular to the natural sedimentary plane. Although R cannot directly reflect the anisotropy of the soil, it can

control the anisotropy through the morphology, physical properties, contact mode, and POGA.

The anisotropy characteristics of undisturbed loess are controlled by the POGA, which was determined by the SEM microphotographs of horizontal and vertical slices at different depths and the ArcGIS standard deviation ellipse. The POGA of the vertical direction in Malan loess is basically parallel to the depositional direction, and a deeper burial depth leads to a more significant result. The azimuth angle range of the POGA in the horizontal directional is approximately 130° – 150° ($N40^\circ W$ – $N60^\circ W$), which may hold some significance for the paleowind direction. Similar studies in other sections of the Loess Plateau are needed to test the robustness of the results obtained herein.

The I_a and H_m parameters are used to characterize the direction of the soil and the order of the grains and aggregates, respectively. Regardless of the vertical or horizontal direction, the I_a of the soil increases with depth, meaning that the directionality of the soil becomes increasingly obvious and the anisotropic characteristics increase. The H_m value changes little with depth in the horizontal direction and decreases with depth in the vertical direction, and the orientation of the grains and aggregates is also better in the vertical direction.

Compared with highly plastic compacted clay, the I_a and H_m show similar changes. When the water content is lower than the threshold value, the anisotropy and order degree increase as the water content increases. When the water content is on the right side of the threshold value, the soil fabric has significant anisotropy and a directional arrangement.

The research method can also be applied for the study of pore characteristics in porous media.

Funding information This research was funded by the Natural Science Foundation China, grant numbers 41572264 and 41877225; the Fundamental Research Funds for the Central Universities, CHD, grant number 300102268717; and the Key Laboratory of Mine Geological Hazards Mechanism and Control, grant numbers KF2017-16 and KF2017-17.

References

- Alan W, Stephen RW, Albert PP (2007) Effect of particle shape on the density and microstructure of random packings. *J Phys Condens Matter* 19:406215
- Al-Rousan T, Masad E, Tutumluer E, Pan T (2007) Evaluation of image analysis techniques for quantifying aggregate shape characteristics. *Constr Build Mater* 21:978–990. <https://doi.org/10.1016/j.conbuildmat.2006.03.005>
- Alshibli KA, Alsaleh MI (2004) Characterizing surface roughness and shape of sands using digital microscopy. *J Comput Civil Eng* 18:36–45. [https://doi.org/10.1061/\(ASCE\)0887-3801\(2004\)18:1\(36\)](https://doi.org/10.1061/(ASCE)0887-3801(2004)18:1(36))
- An ZS, Wu XH, Wang PX, Wang SM, Dong GR, Sun XJ, Zhang DE, Lu YC, Zheng SH, Zhao SL (1991a) The palaeomonsoon in China in recent 130 ka-I. Palaeomonsoon record (in Chinese). *Sci Chin Ser B* 10:1076–1081

- An ZS, Wu XH, Wang PX, Wang SM, Dong GR, Sun XJ, Zhang DE, Lu YC, Zheng SH, Zhao SL (1991b) The paleomonsoon of China in recent 130 ka-II. Paleomonsoon Variations (in Chinese). *Sci Chin Ser B* 11:1209–1215
- Arasan S, Akbulut S, Hasiloglu AS (2011) The relationship between the fractal dimension and shape properties of particles. *KSCE J Civ Eng* 15:1219. <https://doi.org/10.1007/s12205-011-1310-x>
- ArcGis 10.2 (30 July 2013) Environment System Research Institute (ESRI), USA
- Brewer R, Haldane AD (1957) Preliminary experiments in the development of clay orientation in soils. *Soil Sci* 84:301–310
- Cagauan B, Uehara G (1965) Soil anisotropy and its relation to aggregate stability. *Soil Sci Soc Am J* 29:198–200. <https://doi.org/10.2136/sssaj1965.03615995002900020025x>
- Cairncross AM, James RG (1977) Anisotropy in overconsolidated clays. *Géotechnique* 27:31–36. <https://doi.org/10.1680/geot.1977.27.1.31>
- Cetin H (2004) Soil-particle and pore orientations during consolidation of cohesive soils. *Eng Geol* 73:1–11. <https://doi.org/10.1016/j.enggeo.2003.11.006>
- Chapuis RP, Gill DE (1989) Hydraulic anisotropy of homogeneous soils and rocks: influence of the densification process. *Bull Int Assoc Eng Geol* 39:75–86. <https://doi.org/10.1007/BF02592538>
- Cho G-C, Dodds J, Santamarina JC (2006) Particle shape effects on packing density, stiffness, and strength: natural and crushed sands. *J Geotech Geoenviron Eng* 132:591–602. [https://doi.org/10.1061/\(ASCE\)1090-0241\(2006\)132:5\(591\)](https://doi.org/10.1061/(ASCE)1090-0241(2006)132:5(591))
- Cox EP (1927) A method of assigning numerical and percentage values to the degree of roundness of sand grains. *J Paleontol* 1:179–183
- Curtis CD, Lipshie SR, Oertel G, Pearson MJ (1980) Clay orientation in some upper carboniferous mudrocks, its relationship to quartz content and some inferences about fissility, porosity and compactional history. *Sedimentology* 27:333–339. <https://doi.org/10.1111/j.1365-3091.1980.tb01183.x>
- Delage P, Lefebvre G (1984) Study of the structure of a sensitive Champlain clay and of its evolution during consolidation. *Can Geotech J* 21:21–35. <https://doi.org/10.1139/t84-003>
- Ding Z-L, Yu Z-w (1995) Forcing mechanisms of paleomonsoons over East Asia (in Chinese). *Quat Sci* 1:63–74
- Edil TB, Krizek RJ (1975) Quantitative dependence of strength on particle orientation of clay. *Bull Int Assoc Eng Geol* 11:19–22. <https://doi.org/10.1007/BF02635445>
- Graham J, Houlsby GT (1983) Anisotropic elasticity of a natural clay. *Géotechnique* 33:165–180. <https://doi.org/10.1680/geot.1983.33.2.165>
- Hartley CS (1990) Quantitative specification of microstructural anisotropy. *J Phys Colloques* 51:173–177. <https://doi.org/10.1051/jphyscol:1990126>
- Hattab M, Fleureau J-M (2011) Experimental analysis of kaolinite particle orientation during triaxial path. *Int J Numer Anal Methods Geomech* 35:947–968. <https://doi.org/10.1002/nag.936>
- Hattab M, Hammad T, Fleureau J-M, Hicher P-Y (2013) Behaviour of a sensitive marine sediment: microstructural investigation. *Géotechnique* 63:71–84. <https://doi.org/10.1680/geot.13.D.02>
- Henderson N, Pena L (2017) Simulating effects of the permeability anisotropy on the formation of viscous fingers during waterflood operations. *J Petrol Sci Eng* 153:178–186. <https://doi.org/10.1016/j.petrol.2017.03.047>
- Hicher PY, Wahyudi H, Tessier D (2000) Microstructural analysis of inherent and induced anisotropy in clay. *Mech Cohes Frict Mat* 5:341–371. [https://doi.org/10.1002/1099-1484\(200007\)5:5<341::AID-CFM99>3.0.CO;2-C](https://doi.org/10.1002/1099-1484(200007)5:5<341::AID-CFM99>3.0.CO;2-C)
- Hong B, Li XA, Wang L, Li LC (2019) Temporal variation in the permeability anisotropy behavior of the Malan loess in northern Shaanxi Province, China: an experimental study. *Environ Earth Sci* 78:447. <https://doi.org/10.1007/s12665-019-8449-z>
- Hueckel T, Pellegrini R (1996) A note on thermomechanical anisotropy of clays. *Eng Geol* 41:171–180. [https://doi.org/10.1016/0013-7952\(95\)00050-X](https://doi.org/10.1016/0013-7952(95)00050-X)
- Jing C (1980) Climatic Conditions, Times and Genesis of Chinese Loess Formation (in Chinese). *Acta Geogr Sin* 1:83–86
- Karlsson M, Karstunen M (2017) On the benefits of incorporating anisotropy in stability analyses in sensitive clays. In: Thakur V, L'Heureux J-S, Locat A (eds) *Landslides in Sensitive Clays: From Research to Implementation*. Springer International Publishing, Cham, pp 259–266. https://doi.org/10.1007/978-3-319-56487-6_23
- Kock I, Huhn K (2007) Influence of particle shape on the frictional strength of sediments — a numerical case study. *Sediment Geol* 196:217–233. <https://doi.org/10.1016/j.sedgeo.2006.07.011>
- Krumbein WC (1941) Measurement and geologic significance of shape and roundness of sedimentary particles. *J Sediment Petrol* 11:64–72
- Lafeber D (1967) The optical determination of spatial (three-dimensional) orientation of platy clay minerals in soil thin-sections. *Geoderma* 1:359–369. [https://doi.org/10.1016/0016-7061\(67\)90037-7](https://doi.org/10.1016/0016-7061(67)90037-7)
- Lagroix F, Banerjee SK (2002) Paleowind directions from the magnetic fabric of loess profiles in central Alaska. *Earth Planet Sci Lett* 195:99–112. [https://doi.org/10.1016/S0012-821X\(01\)00564-7](https://doi.org/10.1016/S0012-821X(01)00564-7)
- Leroueil S, Bouclin G, Tavenas F, Bergeron L, Rochelle PL (1990) Permeability anisotropy of natural clays as a function of strain. *Can Geotech J* 27:568–579. <https://doi.org/10.1139/t90-072>
- Li HH (1986) The age of Malan loess-II. TL dating of Luochuan section (in Chinese). *Chin Sci Bull* 5:372–375
- Li Y (2013) Effects of particle shape and size distribution on the shear strength behavior of composite soils. *Bull Eng Geol Environ* 72:371–381. <https://doi.org/10.1007/s10064-013-0482-7>
- Li X, Li L (2017) Quantification of the pore structures of Malan loess and the effects on loess permeability and environmental significance, Shaanxi Province, China: an experimental study. *Environ Earth Sci* 76:523. <https://doi.org/10.1007/s12665-017-6855-7>
- Li F, Zhang KY, Luo XJ (2013a) Micro-study of soil's inherent anisotropy with PFC simulation. *Appl Mech Mater* 275-277:383–386. <https://doi.org/10.4028/www.scientific.net/AMM.275-277.383>
- Li Y, Huang R, Chan LS, Chen J (2013b) Effects of particle shape on shear strength of clay-gravel mixture. *KSCE J Civ Eng* 17:712–717. <https://doi.org/10.1007/s12205-013-0003-z>
- Li X, Li L, Song Y, Hong B, Wang L, Sun J (2018) Characterization of the mechanisms underlying loess collapsibility for land-creation project in Shaanxi Province, China—a study from a micro perspective. *Eng Geol* 249:77–88. <https://doi.org/10.1016/j.enggeo.2018.12.024>
- Liang Q, Li J, Wu X, Zhou A (2016) Anisotropy of Q₂ loess in the Baijiapo Tunnel on the Lanyu Railway, China. *Bull Eng Geol Environ* 75:109–124. <https://doi.org/10.1007/s10064-015-0723-z>
- Liu C, Shi B, Zhou J, Tang C (2011) Quantification and characterization of microporosity by image processing, geometric measurement and statistical methods: application on SEM images of clay materials. *Appl Clay Sci* 54:97–106. <https://doi.org/10.1016/j.clay.2011.07.022>
- Liu Z, Liu F, Ma F, Wang M, Bai X, Zheng Y, Yin H, Zhang G (2015) Collapsibility, composition, and microstructure of loess in China. *Can Geotech J* 53:673–686. <https://doi.org/10.1139/cgj-2015-0285>
- Lonardelli I, Wenk H-R, Ren Y (2007) Preferred orientation and elastic anisotropy in shales. *Geophysics* 72:33–40. <https://doi.org/10.1190/1.2435966>
- Lu HY, An ZS (1997) Grain-size composition of Luochuan loess and paleoclimate implication (in Chinese). *Chin Sci Bull* 42(1):66–69
- Lu HY, An ZS (1998) Paleoclimatic significance of grain size of loess-palaeosol deposit in Chinese Loess Plateau (in Chinese). *Sci Chin Ser D* 28(3):278–283
- Magaldi D, Giammatteo M, Smart P (2002) Soil micromorphology of clayey hill slopes, central Italy. *Bull Eng Geol Environ* 61:357–362. <https://doi.org/10.1007/s10064-002-0158-1>

- Manne A, Devarakonda NS (2016) Influence of particle shape and size on the dynamic soil properties. *Jpn Geotech Soc Spec Publ* 2:897–902. <https://doi.org/10.3208/jgssp.IND-08>
- Matalucci RV, Shelton JW, Abdel-Hady M (1969) Grain orientation in Vicksburg Loess. *J Sediment Res* 39:969–979. <https://doi.org/10.2110/jsr.39.909>
- Matalucci RV, Abdel-hady M, Shelton JW (1970a) Influence of microstructure of loess on triaxial shear strength. *Eng Geol* 4:341–351. [https://doi.org/10.1016/0013-7952\(70\)90024-4](https://doi.org/10.1016/0013-7952(70)90024-4)
- Matalucci RV, Abdel-hady M, Shelton JW (1970b) Influence of grain orientation on direct shear strength of a loessial soil. *Eng Geol* 4:121–132. [https://doi.org/10.1016/0013-7952\(70\)90008-6](https://doi.org/10.1016/0013-7952(70)90008-6)
- Meade RM (1965) Mechanics of aquifer system. Removal of water and rearrangement of particles during the compaction of clayey sediments—review: Meade RM 1964. *US Geol Surv Prof Paper* 497-B: 1–22. *Deep Sea Research and Oceanographic Abstracts* 12:1060. [https://doi.org/10.1016/0011-7471\(65\)90996-4](https://doi.org/10.1016/0011-7471(65)90996-4)
- Morgenstern NR, Tchalenko JS (1967a) The optical determination of preferred orientation in clays and its application to the study of microstructure in consolidated kaolin. I. *Proc R Soc Lond Ser A Math Phys Sci* 300:218–234. <https://doi.org/10.1098/rspa.1967.0167>
- Morgenstern NR, Tchalenko JS (1967b) The optical determination of preferred orientation in clays and its application to the study of microstructure in consolidated kaolin. II. *Proc R Soc London Ser A Math Phys Sci* 300:235–250. <https://doi.org/10.1098/rspa.1967.0168>
- Nguyen XP, Cui YJ, Tang AM, Li XL, Wouters L (2014) Physical and microstructural impacts on the hydro-mechanical behaviour of Ypresian clays. *Appl Clay Sci* 102:172–185. <https://doi.org/10.1016/j.clay.2014.09.038>
- Nouguier-Lehon C, Cambou B, Vincens E (2003) Influence of particle shape and angularity on the behaviour of granular materials: a numerical analysis. *Int J Numer Anal Methods Geomech* 27:1207–1226. <https://doi.org/10.1002/nag.314>
- Osipov VI, Sokolov VN (1978) A study of the nature of the strength and deformation properties of clay soils with the help of the scanning electron microscope. *Bull Int Assoc Eng Geol* 17:91–94. <https://doi.org/10.1007/BF02634697>
- Özarslan E, Bassor PJ (2008) Microscopic anisotropy revealed by NMR double pulsed field gradient experiments with arbitrary timing parameters. *J Chem Phys* 128:154511. <https://doi.org/10.1063/1.2905765>
- Pang J-L (1999) Palaeo-monsoon evolution in time and space on the Loess Plateau since the Late Pleistocene (in Chinese). *J Desert Res* 19(1):73–77
- Powers MC (1953) A new roundness scale for sedimentary particles. *J Sediment Petrol* 23:117–119. <https://doi.org/10.1306/D4269567-2B26-11D7-8648000102C1865D>
- Reading HG (Ed.) (1978), Zhou MJ, Chen CM, Zhang J, Pan ZP, Li JY, Shi YT, Su ZW, Li ZQ, Li QF, Xie HY (Transl.) (1985) *Sedimentary environments and facies* (in Chinese). Beijing: Science Press 1985, pp.526
- Rousé PC (2005) Characterisation and modelling of a uniformly graded, well-rounded coarse sand. Thesis/Dissertation, University of British Columbia.
- Rousé PC, Fannin RJ, Shuttle DA (2008) Influence of roundness on the void ratio and strength of uniform sand. *Géotechnique* 58:227–231. <https://doi.org/10.1680/geot.2008.58.3.227>
- Russell RD, Taylor RE (1937) Roundness and Shape of Mississippi River Sands. *J Geol* 45:225–267. <https://doi.org/10.1086/624526>
- Rutter NW (1992) Chinese loess and global change (in Chinese). *Quat Sci* 1:2–11
- Sachan A (2007) Variation in geometric arrangement of particles in kaolinite clay due to shear deformation using SEM technique. *Curr Sci* 93:515–522
- Santamarina JC, Cho GC (2004) Soil behaviour: the role of particle shape. In *Proceedings of Advances in geotechnical engineering: The skempton conference*, London, pp 604–617
- Shi B (1996) Quantitative assessment of changes of microstructure for clayey soil in the process of compaction (in Chinese). *Chin J Geotech Eng* 18(4):60–65
- Shi B, Li S, Tolkachev M (1995) Quantitative approach on SEM images of microstructure of clay soils. *Sci China Ser B* 38:741–748
- Shi B, Murakami Y, Wu Z (1998) Orientation of aggregates of fine-grained soil: quantification and application. *Eng Geol* 50:59–70. [https://doi.org/10.1016/S0013-7952\(97\)00082-3](https://doi.org/10.1016/S0013-7952(97)00082-3)
- Sivakumar V, Doran IG, Graham J (2002) Particle orientation and its influence on the mechanical behaviour of isotropically consolidated reconstituted clay. *Eng Geol* 66:197–209. [https://doi.org/10.1016/S0013-7952\(02\)00040-6](https://doi.org/10.1016/S0013-7952(02)00040-6)
- Sun JM (2004) Provenance, forming mechanism and transport of Loess in China (in Chinese). *Quat Sci* 2:175–183
- Sun JM, Ding ZL, Liu TS, Yuan BY, Guo ZT (1995) A study of loess and paleosol magnetic fabrics on the preliminary application of reconstruction of the winter wind direction (in Chinese). *Chin Sci Bull* 40(21):1976–1978
- Sun DH, An ZS, Liu TS, Wu XH (1996) Evolution of Summer Monsoon at the Loess Plateau during the 150 ka (in Chinese). *Sci Chin Ser D* 26(5):417–422
- Tang Y-Q, Zhou J, Hong J, Yang P, Wang J-x (2012) Quantitative analysis of the microstructure of Shanghai muddy clay before and after freezing. *Bull Eng Geol Environ* 71:309–316. <https://doi.org/10.1007/s10064-011-0380-9>
- Teng ZH, Shen XP (1995) A Study of Eolian Loess and Its Lower Boundary in China (in Chinese). *J Stratigr* 2:81–87
- Ting J, Meachum L, Rowell JD (1995) Effect of particle shape on the strength and deformation mechanism of ellipse shape granular assemblies. *Eng Comput* 12:99–108. <https://doi.org/10.1108/02644409510799497>
- Tovey NK (1973) Quantitative analysis of electron micrographs of soil structure. In *Proceedings of Proceedings International Symposium on Soil Structure*, Gothenburg, Sweden, pp 50–57
- Tovey NK (1980) A digital computer technique for orientation analysis of micrographs of soil fabric. *J Microsc* 120:303–315. <https://doi.org/10.1111/j.1365-2818.1980.tb04150.x>
- Tovey NK, Krinsley DH (1990) A technique for quantitatively assessing orientation patterns in sand grain surface microtextures. *Bulletin de l'Association Internationale de Géologie de l'Ingénieur* 41:117–127. <https://doi.org/10.1007/BF02590212>
- Tovey NK, Krinsley DH (1992) Mapping of the orientation of fine-grained minerals in soils and sediments. *Bull Int Assoc Eng Geol* 46:93–101. <https://doi.org/10.1007/BF02595039>
- Tovey N, Smart P, Hounslow M, Leng XL (1989) Practical aspects of automatic orientation analysis of micrographs. *Scanning Microscopy* 3:771–784
- Tovey NK, Krinsley DH, Dent DL, Corbett WM (1992a) Techniques to quantitatively study the microfabric of soils. *Geoderma* 53:217–235. [https://doi.org/10.1016/0016-7061\(92\)90056-D](https://doi.org/10.1016/0016-7061(92)90056-D)
- Tovey NK, Smart P, Hounslow MW, Leng XL (1992b) Automatic orientation mapping of some types of soil fabric. *Geoderma* 53:179–200. [https://doi.org/10.1016/0016-7061\(92\)90054-B](https://doi.org/10.1016/0016-7061(92)90054-B)
- Wang YY (1987) Paleoclimate change of Quaternary Period in Loess deposits of China. *Sci Chin Ser B* 10:1099–1106
- Wang B (2009) Theories and methods for soil grain orientation distribution in SEM by standard deviational ellipse (in Chinese). *Chin J Geotech Eng* 31(07):1082–1087
- Wang J, Fang X, Zhang Y, Cao J (1995) The anisotropy of loess magnetic susceptibility in the northeastern fringe of Qinghai-Xizang (Tibetan) Plateau as an indicator of palaeowind direction (in Chinese). *J Lanzhou Univ (Nat Sci)* 31(4):155–159

- Wang B, Shi B, Liu Z, Cai Y (2004) Fractal study on microstructure of clayey soil by GIS (in Chinese). *Chin J Geotech Eng* 26(02):244–247
- Wang B, Shi B, Tang C (2007) Study on 3D fractal dimension of clayey soil by use of GIS (in Chinese). *Chin J Geotech Eng* 29(02):309–312
- Wang B, Shi B, Inyang HI (2008a) GIS-based quantitative analysis of orientation anisotropy of contaminant barrier particles using standard deviational ellipse. *Soil Sediment Contam* 17:437–447. <https://doi.org/10.1080/15320380802146784>
- Wang B, Shi B, Cai Y, Tang C (2008b) 3D visualization and porosity computation of clay soil SEM image by GIS (in Chinese). *Rock Soil Mech* 29(01):251–255. <https://doi.org/10.16285/j.rsm.2008.01.049>
- Wang B, Zhang M, Shi B (2010) Quantitative analysis of orientation distribution of soil grains based on slope-aspect theory (in Chinese). *Chin J Rock Mech Eng* 29(S1):2951–2957
- Xu S, Pan B, Gao H, Wang J, Guan Q, Hu C (2006) Analysis of grain-size populations with environmentally sensitive components of loess during the last interglacial-glacial cycle and their implications (in Chinese). *Acta Pedologica Sin* 43(2):183–189
- Xu J, Li Y, Yang X (2018) Stability charts and reinforcement with piles in 3D nonhomogeneous and anisotropic soil slope. *Geomech Eng* 14: 71–81. <https://doi.org/10.12989/gae.2018.14.1.071>
- Zevin L, Viaene W (1990) Impact of clay particle orientation on quantitative clay diffractometry. *Clay Miner* 25:401–418. <https://doi.org/10.1180/claymin.1990.025.4.01>
- Zhang X-Y (2001) Source distributions, emission, transport, deposition of Asian dust and Loess accumulation (in Chinese). *Quat Sci* 211(1): 29–40
- Zhang R, Kravchinsky VA, Zhu R, Yue L (2010) Paleomonsoon route reconstruction along a W-E transect in the Chinese Loess Plateau using the anisotropy of magnetic susceptibility: summer monsoon model. *Earth Planet Sci Lett* 299:436–446. <https://doi.org/10.1016/j.epsl.2010.09.026>
- Zhang W-Y, Luo C-Q, Han J, Wu W-J, Ma Y-X, Chang L-J (2017) Experimental study on the micro-mechanism for strength anisotropy of intact loess. In *Proceedings of 2017 International Conference on Transportation Infrastructure and Materials (ICTIM 2017)*, DEStech Publications, Inc., pp 742–751.
- Zhao J-B, Yue Y-L, Du J (2002) Formation of Loess and division of climate cycles (in Chinese). *J Desert Res* 22(1):11–15
- Zhao X, Zhang C, Luan Y, Xiao Z (2018) Stereological analyses of microstructure of granular soils using the numerical method. *Bull Eng Geol Environ* 77:1103–1115. <https://doi.org/10.1007/s10064-017-1086-4>